Interface Recombination in Ga- and N-Polar GaN/(Al,Ga)N Quantum Wells Grown by Molecular Beam Epitaxy

T. Auzelle,[1,*] C. Sinito,[1,2] J. Lähnemann,[1] G. Gao,[1,3] T. Flissikowski,[1] A. Trampert,[1] S. Fernández-Garrido,[1,4] and O. Brandt[1]

[1] *Paul-Drude-Institut für Festkörperelektronik, Leibniz-Institut im Forschungsverbund Berlin e. V., Hausvogteiplatz 5–7, Berlin 10117, Germany*

[2] *Present address: WILCO AG, Rigackerstrasse 11, Wohlen 5610, Switzerland*

[3] *Present address: Materials Science and Nano-engineering Department, Rice University, Houston, Texas 77005, USA*

[4] *Grupo de Electrónica y Semiconductores, Dpto. Física Aplicada, Universidad Autónoma de Madrid, Madrid 28049, Spain*

(Received 25 November 2021; revised 21 February 2022; accepted 22 March 2022; published 15 April 2022)

We explore and systematically compare the morphological, structural, and optical properties of GaN/(Al,Ga)N multiple quantum wells (MQWs) grown by plasma-assisted molecular beam epitaxy (PA MBE) on freestanding GaN(0001) and GaN(000$\bar{1}$) substrates. Samples of different polarity are found to be comparable in terms of their morphological and structural perfection and exhibit essentially identical quantum well widths and Al content. Regardless of the crystal orientation, the exciton decay in the MQWs at 10 K is dominantly radiative and the photoluminescence (PL) energy follows the quantum confined Stark effect for different quantum well widths. A prominent free-to-bound transition involving interface shallow donors is, however, visible for the N-polar MQWs. At room temperature, in contrast, the exciton decay in all samples is dominated by nonradiative recombination taking place at point defects, presumably Ca or V_N located at the bottom QW interface. Remarkably, the N-polar MQWs exhibit a higher PL intensity and longer decay times than the Ga-polar MQWs at room temperature. This improved internal quantum efficiency is attributed to the beneficial orientation of the internal electric field that effectively reduces the capture rate of minority carriers by interface trap states.

DOI: 10.1103/PhysRevApplied.17.044030

I. INTRODUCTION

The adverse effect of dislocations on the internal quantum efficiency of GaN/(Al,Ga)N heterostructures can be essentially resolved by reducing the dislocation density below 5×10^7 cm^{-2} [1,2], a regime directly attainable for growth on freestanding GaN or AlN substrates. Nonradiative processes in these heterostructures are thus mediated by nonradiative point defects [3,4], whose density must be lowered to reach high luminous efficiencies. In this regard, optimization of the III:V ratio or Si doping have been reported to enhance the internal quantum efficiency of metal polar (Al,Ga)N quantum wells (QWs) grown by metalorganic chemical vapor deposition (MOCVD) [5,6]. Yet, establishing other strategies to further decrease the density of point defects in GaN/(Al,Ga)N heterostructures would certainly benefit to the performance of nitride-based ultraviolet light emitters [7], transistors [8–11], and future devices. For the epitaxial growth of semiconductors, it is well known that the crystal orientation influences not only the surface morphology [12–16], but also the incorporation of impurities and the formation of nonradiative point defects [17–19]. For instance, a dramatic case is (In,Ga)N/GaN QWs grown by plasma-assisted molecular beam epitaxy (PA MBE), which may not exhibit any detectable luminescence even at 10 K if grown N-polar [i.e., on GaN(000$\bar{1}$)] instead of Ga-polar [i.e., on GaN(0001)] [20,21]. The origin of this phenomenon is related to the presence of nonradiative defects at the QW-barrier interface. A potential candidate for this as yet unknown point defect is the impurity Ca [22,23], which can contaminate the substrate surface during wet cleaning and gradually incorporates in the overgrown nitride layers [24].

Growth of GaN/(Al,Ga)N heterostructures on various crystal orientations has been already reported by MBE [25–30] and MOCVD [31–35], but a systematic investigation of the impact of crystal orientation on the incorporation rate of nonradiative point defects is still lacking. A particular interest lies in the (000$\bar{1}$) orientation since

*auzelle@pdi-berlin.de

it exhibits internal electric fields of opposite direction compared to the classical (0001) orientation, which is seen as favorable for improving the efficiency of high-frequency transistors [36], light-emitting diodes [37–40], and solar cells [41]. Lastly, the $(000\bar{1})$ orientation is currently available in the form of freestanding GaN substrates at similar costs than the classical (0001) ones and is also the usual growth direction of dislocation-free GaN nanowires obtained by self-assembly [42].

In this work, we systematically compare the morphological, structural, and optical properties of (0001) and $(000\bar{1})$ GaN/(Al,Ga)N multiple quantum wells (MQWs) grown by PA MBE and discuss the observed differences in terms of point defect incorporation at the bottom QW interface. As a prerequisite, the samples of different polarity are first evidenced to be comparable in terms of their morphological and structural perfection. Low concentrations of impurities are found, with the exception of Ca, whose concentration is seen to be high in the Ga-polar samples, 10 times higher than for the N-polar samples. For all the MQWs, the low-temperature photoluminescence (PL) shows a predominantly radiative behavior, whereas the room-temperature PL is dominated by nonradiative interface recombination. However, the N-polar MQWs exhibit an improved internal quantum efficiency at room temperature in comparison to the Ga-polar MQWs, an effect that originates from the opposite direction of the internal electric field.

II. EXPERIMENTS AND METHODS

The MQWs samples under investigation consist of the layer sequence sketched in Fig. 1. They are grown in a PA-MBE setup equipped with a Veeco plasma cell to generate active N and effusion cells for Ga and Al. The atomic fluxes are calibrated by growing thick GaN(0001) and AlN(0001) layers as described in Ref. [43]. Freestanding GaN is chosen as the substrate to nominally provide

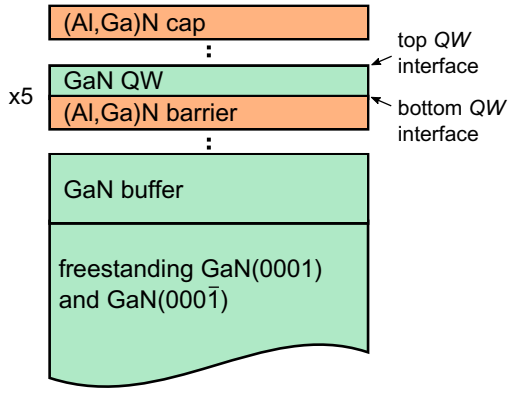

FIG. 1. Nominal structure of the series of GaN/(Al,Ga)N MQWs under investigation. The growth of the GaN and (Al,Ga)N layers is repeated five times (x5) to form five QWs.

equivalent structural quality for Ga- and N-polar samples. The substrates were purchased from Suzhou Nanowin Science and Technology, with a nominal threading dislocation density below 5×10^6 cm^{-2} and a $0.35° \pm 0.15°$ miscut toward the $[1\bar{1}00]$ direction. The in-house substrate preparation consists of a 5 min dip in a 5% hydrogen fluoride solution before mounting them with In on a 2" in. GaN/Al_2O_3 template backside coated with Ti. They are next degassed in vacuum for 20 min at 300 °C and *in situ* cleaned right before growth by a sequence of Ga deposition and desorption steps at approximately 600 and 750 °C, respectively. This preparation is aimed at reducing the amount of residues on the GaN surface to prevent the formation of extended defects at the regrowth interface [44–47]. Next, an approximate 600-nm-thick buffer of GaN is grown in order to bury the residual impurities located on the substrate surface. Nominal atomic fluxes of 5.7×10^{14} s^{-1} cm^{-2} for N and 8.5×10^{14} s^{-1} cm^{-2} for Ga are used, corresponding to a Ga surplus of 50% relative to the N flux, which should ensure a smooth growth for both polarities [48]. The growth is N limited, resulting in a growth rate of 7.7 nm/min. The substrate temperature is constantly tuned to set the growth conditions at the boundary below which Ga will start accumulating on the surface as droplets [43,49]. This is checked by monitoring the intensity change of the reflection high-energy diffraction pattern, which dims in the presence of metal droplets. This way, the growth conditions are optimized for each sample, independently of their polarity and of their thermal contact with the substrate holder. Based on the growth diagrams of Refs. [43,49], the effective substrate temperature amounts to 700 ± 10 and 715 ± 10 °C for the Ga-polar and N-polar samples, respectively. The difference results from the slightly larger activation energy for desorption of Ga adatoms on the $GaN(000\bar{1})$ surface (3.1–3.6 eV [49,50]) compared to the GaN(0001) one (2.8–3.2 eV [50,51]). Prior to the first (Al,Ga)N barrier growth, the substrate temperature is nominally fixed and the Ga surplus relative to the N flux is reduced to 30%. This is to ensure the absence of metal accumulation when the Al flux is additionally provided for the (Al,Ga)N barrier growth. Then, the heterostructure is grown only by sequentially opening and closing the Al cell shutter, using a nominal atomic flux of 0.8×10^{14} s^{-1} cm^{-2}. No growth interruptions have been performed to smooth the interfaces. The low growth temperature used here should prohibit exchanges between Ga and Al atoms during capping of the GaN QWs by the (Al,Ga)N barrier [52,53]. Hence, the growth rates of the GaN quantum wells and (Al,Ga)N barriers are limited by the N flux, and the Al content within the (Al,Ga)N barriers corresponds to the Al:N ratio [54]. Two series of Ga- and N-polar MQWs are grown, by varying the thickness of the GaN QWs. Their structural parameters are gathered in Table I. Widths are indicated in nanometers and in monolayers (MLs), where a GaN ML amounts to

TABLE I. Structural properties of the investigated samples as deduced from the x-ray analysis. The widths are denoted both in monolayers (MLs) and in nanometers and have an uncertainty of 1 ML related to the inhomogeneity over the sample.

Polarity	GaN QWs width	(Al,Ga)N barrier width	(Al,Ga)N capping layer width	Al content (%)
Ga	10 ML (2.59 nm)	30 ML (7.75 nm)	126 ML (32.55 nm)	8.9
N	10 ML (2.59 nm)	30 ML (7.75 nm)	126 ML (32.55 nm)	8.9
Ga	17 ML (4.41 nm)	30 ML (7.75 nm)	126 ML (32.55 nm)	8.9
N	17 ML (4.41 nm)	29 ML (7.49 nm)	124 ML (32.03 nm)	8.7
Ga	23 ML (5.96 nm)	30 ML (7.75 nm)	126 ML (32.55 nm)	8.8
N	22 ML (5.70 nm)	29 ML (7.49 nm)	123 ML (31.76 nm)	10.2

0.259 nm and an $Al_{0.1}Ga_{0.9}N$ ML 0.258 nm. To ensure comparable growth conditions, pairs of Ga- and N-polar samples with similar structures are grown the same day, in two subsequent runs.

Once grown, the samples are structurally and morphologically characterized by atomic force microscopy (AFM) using the PeakForce Tapping mode of Bruker's Dimension Edge and x-ray diffraction (XRD) carried out in a PANalytical X'Pert Pro diffractometer equipped with a Ge(220) hybrid monochromator, using the $Cu_{K\alpha_1}$ radiation (wavelength $\lambda = 1.54056$ Å). Symmetric $\omega - 2\theta$ scans across the 0002 GaN Bragg reflection are carried out with an open detector (without crystal analyzer or slit) and the experimental diffraction scans are simulated using a dynamical x-ray diffraction model [55]. Transmission electron microscopy (TEM) is additionally performed on a pair of Ga- and N-polar samples to get local insight into the interface structure of the heterostructure. Cross sections are prepared by mechanical grinding and Ar-ion beam milling down to electron transparency. Measurements are performed at 200 kV in a Jeol 2100F field emission microscope, equipped with a Gatan Ultra Scan 4000 CCD.

Impurity concentrations are measured by secondary ion mass spectrometry (SIMS) measurements performed by RTG Mikroanalyse GmbH Berlin. O and C atoms are measured in a Cameca IMS 4s setup using a primary Cs^+ ion source. B and Ca atoms are measured in a Cameca IMS 4fe6 setup using a primary O_2^+ ion source. Quantification of the SIMS signal is done by measuring ion implanted standards. Care is taken to check that the measured ^{40}Ca signal does not include any contributions from compounds such as $^{28}Si^{12}C$ and $^{24}Mg^{16}O$.

Continuous-wave (cw) PL spectroscopy is performed with the 325 nm line of a He-Cd laser and the 244 nm line of a frequency-doubled Ar ion laser. The PL signal is collected in backscatter geometry and dispersed by an 80 cm monochromator and detected by a charge-coupled device (CCD) detector cooled with liquid N. The measurements are corrected for the spectral response of the setups. Time-resolved (TR) PL is carried out using the second harmonic of femtosecond pulses obtained from an optical parametric oscillator pumped by a Ti:sapphire laser. The emission wavelength and the repetition rate are 325 nm and 76 MHz, respectively, and the energy fluence per pulse is maintained below 0.2 $\mu J/cm^2$. The transient emission is spectrally dispersed by a monochromator and detected by a streak camera. Both for cw PL and TR PL, the samples are mounted together on a cold-finger cryostat allowing measurements at 10 K.

The band profiles and wave functions are computed using a one-dimensional (1D) Schrödinger-Poisson solver [56], using similar parameters as in Ref. [21].

III. RESULTS AND DISCUSSION

A. Morphological and structural characterization

Figure 2 shows representative AFM images from the Ga- and N-polar 10 ML MQWs. Both samples feature a smooth surface with a root-mean-square (rms) roughness

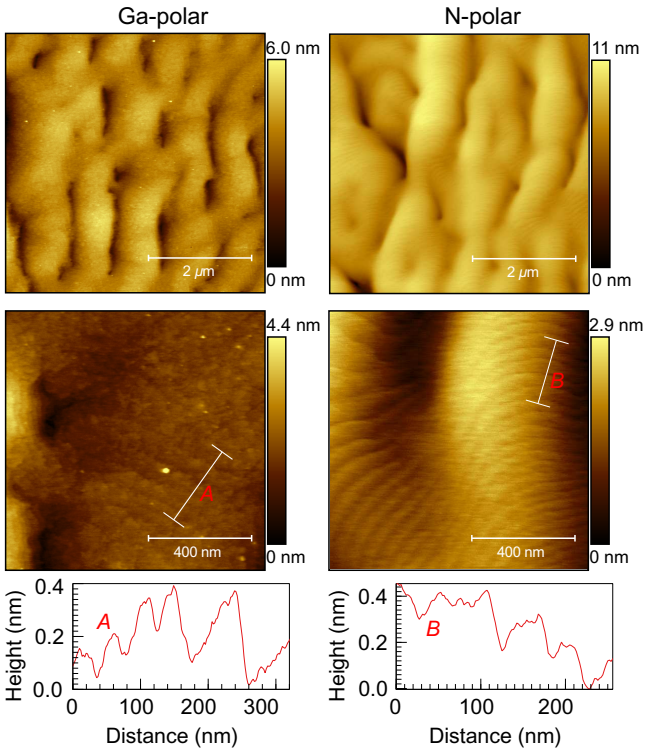

FIG. 2. Representative AFM images of the pair of Ga-polar and N-polar 10 ML GaN/(Al,Ga)N MQWs. Linescans *A* and *B* show atomic steps with a step height of 1–2 ML.

below 1.5 nm. Hillocks related to mixed-type dislocations [57] are not visible here, in agreement with the nominal substrate density of threading dislocations (approximately 5×10^6 cm^{-2}). A step-flow growth mode is confirmed by the presence of clear atomic steps with a step height equal to 1–2 ML. However, a pronounced meandering of the terrace edges is observed, resulting in few nanometer deep trenches, which causes the rms roughness value to exceed 1 nm. This fingerlike morphology typically arises during the epitaxy of N-polar nitride layers in metal-rich conditions [48,58–60] and also for the growth of Ga-polar GaN layers in specific conditions (e.g., at 780 °C with a large III:V ratio of 1.6 [61]). The meanders form as a result of a large Ehrlich-Schwöbel barrier at the kinks of the step edges that makes adatom diffusion along step edges asymmetric and favors kink bunching [62].

Figure 3 displays representative symmetric $\omega - 2\theta$ scans acquired across the 0002 GaN Bragg reflection with an open detector, thus resembling a rocking curve. Superlattice satellites and pronounced interference fringes related to the MQW structure are equally visible for both sample polarities. The entire profiles are in excellent agreement with those expected theoretically despite the absence of a crystal analyzer. The minimal broadening and damping is attributed to the absence of dislocation-induced strain [63] and to an excellent spatial uniformity of the heterostructure. We note that in this diffraction configuration, the effect of interface roughness (with a rms value ≤ 2 ML) on the diffraction pattern is very small. The experimental diffraction profiles are fitted by simulating GaN/(Al,Ga)N MQWs following two constraints: (1) only complete monolayers are considered and (2) the atomic fluxes are assumed constant during the full heterostructure growth (i.e., equal widths for all the quantum wells of a single heterostructure). Optimum fits for the diffraction profiles of the pair of 10 ML MQWs are shown in Fig. 3. The structural parameters obtained from the optimum fits of all the samples are provided in Table I. The error bars are set to 1 ML to account for the fit accuracy and the dispersion within each sample. The N-polar heterostructures are seen on average slightly thinner than their Ga-polar counterparts, in agreement with the observations of Okamura *et al.* [49], who reported a lower efficiency for the incorporation of N adatoms on the GaN(000$\bar{1}$) surface compared to the GaN(0001) one. Beside these small differences, the Ga- and N-polar samples appear structurally equivalent.

TEM analysis of a pair of Ga-polar (23 ML) and N-polar (22 ML) MQWs is performed to get local insights into the heterostructures. Typical micrographs are shown in Fig. 4. The low amount of Al in the (Al,Ga)N barriers leads to a weak contrast, but the full heterostructure remains visible for both samples. The QWs are seen to all be equivalent for each sample and with widths in full agreement with the x-ray predictions. No extended defects

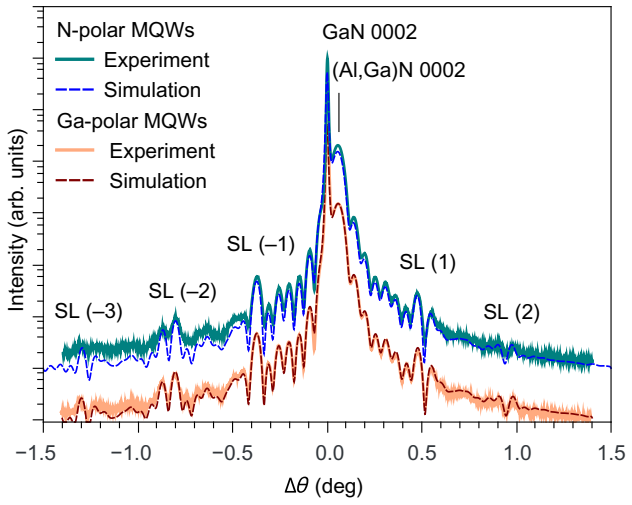

FIG. 3. Representative symmetric $\omega - 2\theta$ scans across the 0002 GaN Bragg reflection of the pair of Ga- and N-polar 10 ML GaN/(Al,Ga)N MQWs. The simulated diffraction profiles for GaN/(Al,Ga)N MQWs resulting in the optimum fit of the experimental data are superposed. Superlattice satellites (SLs) are labeled and the diffraction profiles are vertically shifted for clarity.

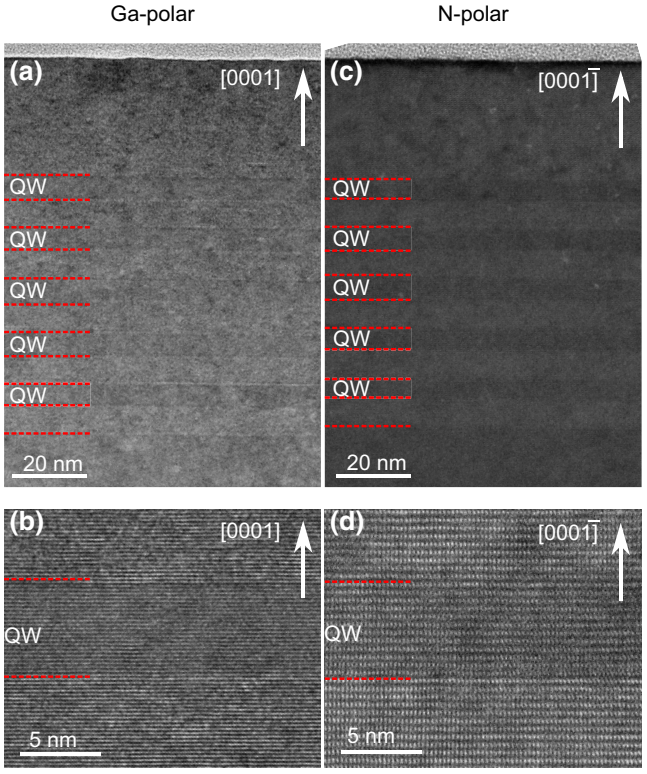

FIG. 4. TEM micrographs of Ga-polar (a),(b) and N-polar (c),(d) 23/22 ML GaN/(Al,Ga)N MQWs. (b),(d) Magnified micrographs over one quantum well of the stack. The dotted lines are guides to the eye to locate the GaN/(Al,Ga)N interfaces. Panels (a) and (b) are taken in the [1$\bar{1}$00] zone axis and (c) and (d) are taken in the [11$\bar{2}$0] zone axis.

such as stacking faults, inversion domains, or dislocations can be seen. The limited contrast between the GaN and the (Al,Ga)N layers prevents a quantitative analysis of the interface roughness. For comparison purposes, Sarigiannidou *et al.* [25] reported by TEM chemically abrupt interfaces at the monolayer scale for both Ga- and N-polar GaN/AlN MQWs grown at 720 °C by PA MBE without growth interruptions. The absence of intermixing was also inferred by atom probe tomography [64,65], with the exception of the early work of Mazumder *et al.* [28]. Therefore, no drastic increase in the interface roughness for N-polar MQWs compared to Ga-polar MQWs should be expected here.

The combination of AFM, x-ray diffraction, and TEM analysis evidences an excellent and equivalent structural quality for the pairs of Ga- and N-polar GaN/(Al,Ga)N MQWs. The absence of extended defects allows us a direct investigation of the nonradiative processes mediated by point defects within the heterostructure.

B. Impurity concentration

Elemental depth profiles using SIMS are used to measure and compare the concentration of C, O, B, and Ca impurities incorporated in the pair of Ga- and N-polar 10 ML MQWs. The results are shown in Fig. 5. The Al signal is used to locate the substrate, the GaN buffer, and the actual GaN/(Al,Ga)N heterostructure along the depth profile. The parasitic incorporation of Al in the GaN buffer is attributed to the high beam equivalent pressure of N_2, dragging atoms from transversing molecular beams to the substrate analogous to the As drag effect [66]. For all impurities, a surface peak is observed that corresponds to surface contamination and is thus further neglected.

C, O, and B, which are the contaminants typically considered for GaN grown by PA MBE, are seen with very low levels, down to (2–3) $\times 10^{16}$ cm^{-3} for C and O, and down to (7–8) $\times 10^{16}$ cm^{-3} for B in the GaN buffer, which is at the very bottom range for GaN grown by MBE [44,60,67–70]. Interestingly, the N-polar layer exhibits the same amounts of C and O as the Ga-polar one, which is in contrast with some reports dealing with MBE growth [20,44,70,71] or HVPE growth [19] but agrees with some others [49,60,68]. By comparing the substrates and methods used in these different works, it appears that growing the Ga- and N-polar samples in different runs instead of a single one is crucial to obtain equally low impurity incorporation in both polarities. The optimum growth conditions for Ga- and N-polar GaN thus differ. In a more general manner, it follows from these works that impurity incorporation can be readily decreased to very low levels independent of the polarity by minimizing the concentration of extended defects [72], by growing at optimized conditions close to stoichiometry and by minimizing the residues on the substrates surface prior to growth [46].

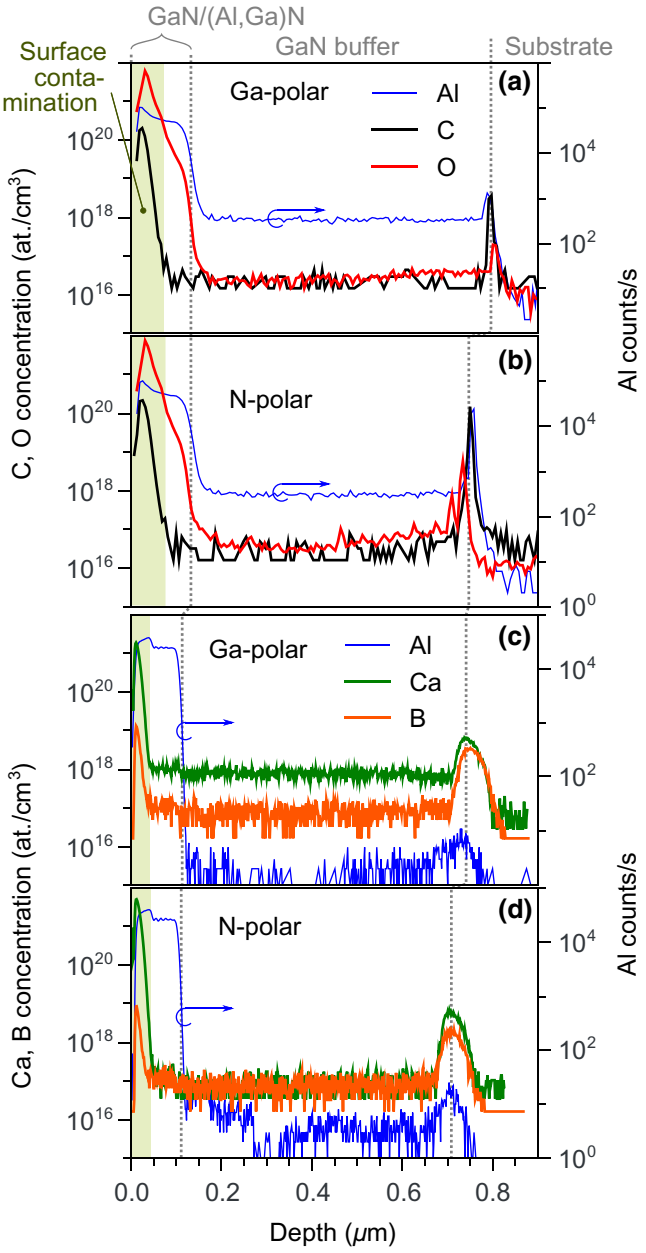

FIG. 5. SIMS analysis performed on the Ga- and N-polar 10 ML GaN/(Al,Ga)N MQWs. (a),(b) O and C elemental depth profiles acquired using a primary Cs^+ ion source; (c),(d) Ca and B elemental depth profiles acquired using a primary O_2^+ ion source. The Al signal is used as a marker and is not quantified.

Larger concentrations of O and C are observed at the regrowth interface of the N-polar sample compared to the Ga-polar one, which agrees with the usual statement that the GaN(000$\bar{1}$) surface has a thicker native oxide compared to the GaN(0001) surface [73] owing to a larger reactivity of the bare surface toward O [74].

If not complexed to other point defects, C, O, and B are not expected to act as nonradiative centers in nitrides and can be further disregarded [75,76]. In contrast, following

the work of Young *et al.* [24], Ca appears as a common impurity in MBE grown nitrides, potentially acting as a strong nonradiative recombination center [22]. Ca is expected to stem from the substrate surface and to segregate on the growth front where it gradually incorporates in the layer, at higher rates for lower growth temperatures. Fairly high amounts of Ca are detected in the Ga- and N-polar GaN buffers of the investigated samples, with respective concentrations of 8×10^{17} and 8×10^{16} cm^{-3}. We recall that these layers were grown at about 700 and 715 °C, respectively. Chèze *et al.* [23] have also reported a slightly larger Ca concentration of (3–5) $\times 10^{17}$ cm^{-3} for a N-polar GaN buffer grown by PA MBE at 730 °C, whereas Young *et al.* [24] found only 8×10^{15} cm^{-3} of Ca impurities in a Ga-polar GaN buffer grown by NH_3 MBE at 820 °C. Hence, in addition to the growth temperature [24], the Ca incorporation rate appears to be drastically affected by the MBE growth method and the crystal orientation. Here, unlike in Ref. [24], the reservoir of Ca at the growth front does not deplete after growth of several hundreds of nanometers of GaN with a Ca concentration above 5×10^{17} cm^{-3}. This finding indicates a comparatively large amount of Ca initially present at the substrate surface prior the growth (> 0.1 ML), which likely originates from the chemomechanical polishing of the freestanding GaN substrates used here and also in the study of Chèze *et al.* [23].

In the GaN/(Al,Ga)N heterostructures, the impurity concentration is seen to increase by 25%, as compared to the GaN buffers for Ca and B atoms. Note that the large increase of the signal close to the surface corresponds to surface contamination. In the case of O, the large surface-related signal prevents an unambiguous determination of the O content in the heterostructure. It is likely that the presence of Al triggers the observed increased levels of Ca and B impurities within the heterostructures, as already reported for O incorporation during growth of (Al,Ga)N [69] or III-As [77,78].

In conclusion, with the exception of Ca, equally low concentrations of impurities are found in the pair of Ga- and N-polar samples. So far, Ca has been reported to act as a nonradiative center for the (In,Ga)N/GaN system, but the question remains open in the case of GaN/(Al,Ga)N.

C. Low-temperature photoluminescence

The cw-PL spectra acquired at 10 K for the series of Ga- and N-polar MQWs are shown in Figs. 6(a)–6(c), along with the extracted energy and width of the observed PL bands. Besides the GaN buffer signal at 3.47 eV, the MQW PL appears as a broad band accompanied by several phonon replica of lower intensity. Fine structures are visible in each of the bands and are assigned to the localization of holes at the GaN/(Al,Ga)N interface of the MQWs [64,79–82]. Only a weak PL signal related to the (Al,Ga)N barriers is observed at 3.65 eV (not shown here). Remarkably, it can be seen that the Ga-polar samples exhibit a single PL band whereas the N-polar samples systematically exhibit a doublet. The splitting between the high- and low-energy bands increases from 25 to 51 meV, from the narrower to the wider MQWs. The laterally spatially uniform origin of the doublet is confirmed by low-temperature monochromatic cathodoluminescence maps of the N-polar 22 ML MQW surface (not shown here).

Transients of the PL bands of the various MQWs are plotted in Figs. 6(d)–6(f). The lifetimes are extracted by fitting monoexponential decays, with the exception of the low-energy band of the N-polar 10 ML MQW, for which a biexponential decay is used to account for the overlapping signal from the GaN buffer (fast component with a typical decay time of 0.4–0.6 ns). Since the acquisition interval is too short to capture the entire decay of the low-energy band of the N-polar MQWs [Fig. 6(f)], the corresponding error bars are larger than for the high-energy band. The partial spectral overlap between the high- and low-energy bands of the N-polar samples is responsible for the slow component showing up in the transient of the high-energy band of the N-polar 10 ML MQWs. This slow component is neglected in the following. The extracted lifetimes are plotted in Fig. 6(g) and show a monotonic increase for wider MQWs. The increase agrees with the decrease in the electron and hole wavefunctions overlap due to the internal electric field [83] and thus shows the dominance of radiative recombination.

In order to identify the contribution of the quantum confined Stark effect (QCSE) in the MQWs PL energy and width, 1D Schrödinger-Poisson calculations for the Ga- and N-polar MQWs are performed. The structural parameters of Table I and a residual donor concentration of 5×10^{16} cm^{-3} are used to simulate the heterostructures. Half of the theoretical value of the polarization coefficients are used since they provide a better agreement with experiments reported so far [84]. The Fermi level energy at the sample surface is set to 0.8 eV below the conduction band, as reported for as-grown Ga-polar $Al_{0.1}Ga_{0.9}N$ [85]. The same value is used for Ga- and N-polar heterostructures since there are no reports for this quantity for N-polar (Al,Ga)N. The calculation outputs the band profile and the internal electric field of the heterostructure. Exemplary results are shown in the Appendix (Fig. 8) for the 23/22 ML GaN/(Al,Ga)N MQWs. In addition, the calculations deliver single-particle transitions for each of the QWs of the heterostructure, which is used as an estimate for the PL energy of the MQWs (excitonic effects are ignored). Each QW of the same heterostructure has a different environment (e.g., distance to the surface) that leads to a different amplitude of their internal electric field. The differences in the single-particle transition energies for the five QWs of each sample are then used as an estimate of the full width at half maximum of the MQW's PL signal.

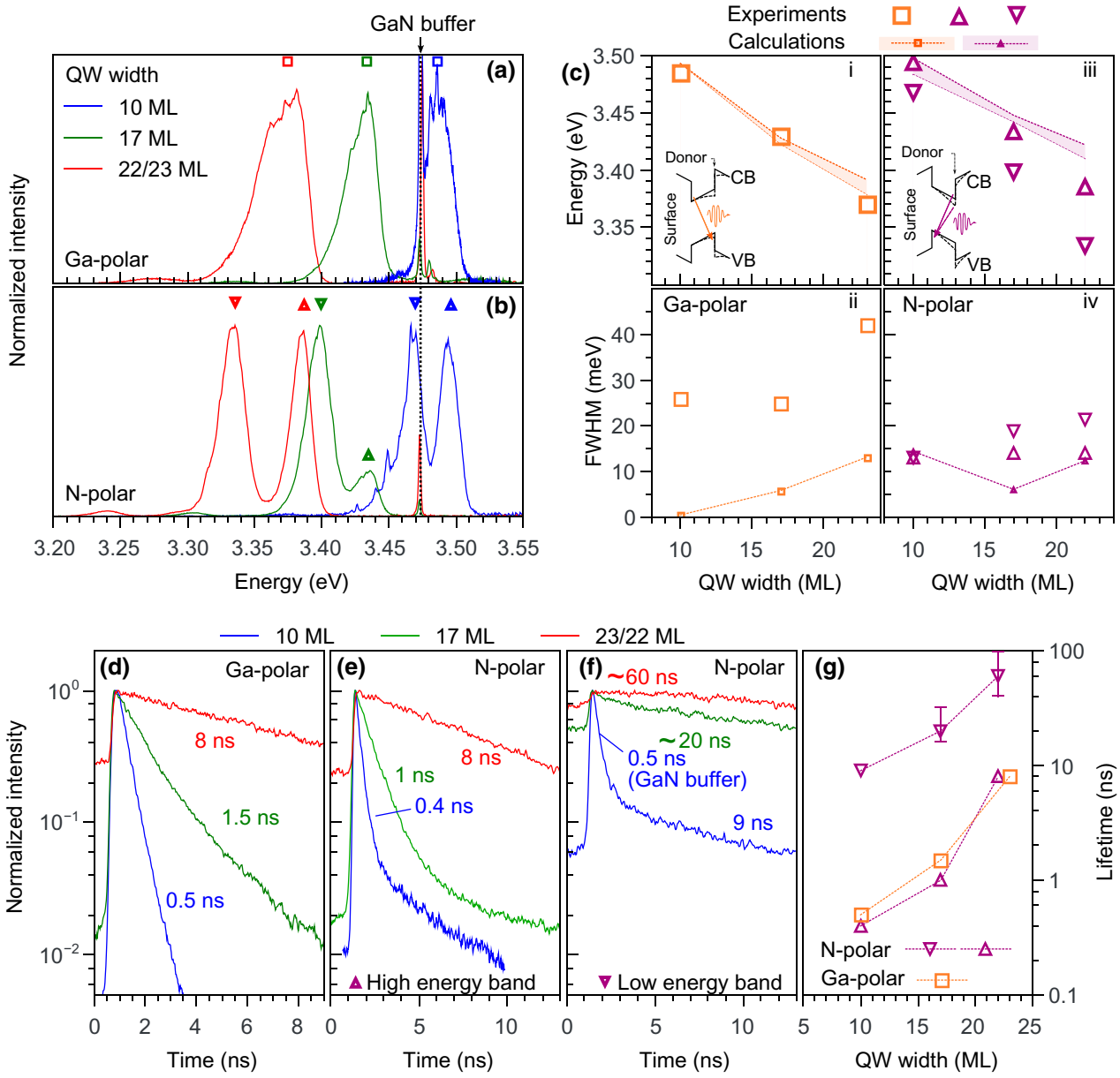

FIG. 6. The 10 K PL of the three pairs of GaN(Al,Ga)N MQWs. (a),(b) Normalized cw-PL spectra acquired with an excitation density of 600 W/cm^2 at 325 nm. (c) Energy and FWHM of the cw-PL band stemming from the MQWs. Dotted lines are results from the 1D Schrödinger-Poisson calculations. The shaded areas in i and ii depict the calculated spread in the electron-hole energy separation between the five QWs of the heterostructure. The dotted (plain) band profiles shown in the insets in i and iii schematically depict the modification of the potential profile in the presence (absence) of an ionized donor located at the bottom interface of the QW. CB and VB refer to the conduction and valence bands, respectively. (d)–(f) PL transients of the three pairs of GaN/(Al,Ga)N MQWs. (g) Plot of the extracted lifetimes versus the QW width.

For the Ga-polar samples, excellent agreement is found between the calculated and experimental PL energies, as shown in Fig. 6(c). Only the calculated FWHMs are underestimated, which can be attributed to the alloy disorder in the (Al,Ga)N barriers, to the random positions of ionized dopants [86] and to monolayer fluctuations in the QW widths [26,80]. According to the calculations, the internal electric field within the GaN QWs amounts to 280 ± 50 kV/cm. Since the recombination energy and rate of the Ga-polar MQWs at 10 K can be entirely ascribed to the presence of the internal electric field, we then conclude that the exciton decay within the MQWs is predominantly radiative, as typically reported for high-quality Ga-polar GaN/(Al,Ga)N heterostructures [87,88].

For the N-polar samples, the calculated PL energies match well the high-energy band, but largely overestimate

the low-energy band. The calculated FWHMs also underestimate the experimental values, likely for the same reasons invoked for the Ga-polar samples. The internal electric field amounts to 170 ± 40 kV/cm, which is lower than for the Ga-polar QWs. This reduction is attributed to the surface band bending since in the N-polar (Ga-polar) case, its electric field is opposed (aligned) to that generated by the spontaneous and piezoelectric polarizations. In analogy to the Ga-polar case, we attribute the high-energy PL band of the N-polar MQWs to a predominantly radiative excitonic recombination dominated by the QCSE.

Concerning the low-energy PL band, we consider several different scenarios. First, the widths of GaN/(Al,Ga)N QWs are commonly observed to fluctuate by ± 2 ML, potentially giving rise to multiple excitonic features in the PL spectra [26,89,90]. Yet, according to Fig. 6(c), a net increase in the QW width of $+4$ ML is required to account for the 50 meV splitting between the PL band of the wider N-polar MQWs. Our XRD and TEM data (cf. Figs. 3 and 4) do not exhibit any evidence for such a large thickness fluctuation. In addition, the PL spectra do not show any signal associated with QW widths of $+1$, $+2$, and $+3$ ML, as would be expected for a GaN/(Al,Ga)N interface with such a degree of roughness. Furthermore, the exceptionally long decay time of the low-energy as compared to the high-energy band could not be explained by recombination of excitons in a QW wider by a few MLs only.

Second, an even larger splitting between transitions of $Al_{0.7}Ga_{0.3}N/Al_{0.6}Ga_{0.4}N$ MQWs grown by MOCVD has been attributed to biexcitons with an extraordinarily large binding energy [91]. However, much lower biexciton binding energies have been observed in GaN/(Al,Ga)N QWs with low Al content [92]. For the 9% Al content corresponding to our samples, a biexciton binding energy of only 2 meV is expected for a well width of 10 ML, and even lower values are extrapolated for thicker wells due to the impact of the internal electric fields in QWs with a width exceeding the exciton Bohr radius [93]. In addition, we have performed excitation-density-dependent measurements (not shown here) that reveal the low-energy line to saturate for higher excitation densities, suggesting that this line is associated with an impurity rather than being of intrinsic origin.

Third, bound excitons are an excitonic complex analogous to the biexciton, but tied to an impurity. The donor-bound exciton usually dominates the PL spectra of bulklike GaN and has a binding energy of 6–7 meV. He *et al.* [94] attributed a splitting of about 60 (90) meV in the PL spectra of $Al_{0.5}Ga_{0.5}N/Al_{0.35}Ga_{0.65}N$ MQWs grown by MOCVD to the recombination of Si (O) donor-bound excitons. However, such a large splitting is inconceivable in a GaN QW. The maximum donor ionization energy in $GaN/Al_{0.15}Ga_{0.85}N$ QWs has been calculated to be 60 meV [86], which translates into a binding energy of the donor-bound exciton of 12 meV, much too small to account for the splitting experimentally observed.

The donor ionization energy itself, however, is close to this splitting. Lastly, we thus consider the radiative recombination between a shallow donor (such as O) and a free hole. Free-to-bound recombination is commonly observed in doped GaAs/(Al,Ga)As heterostructures [95] but has been scarcely considered in GaN/(Al,Ga)N heterostructures. However, in a GaN/(Al,Ga)N-based QW with a width exceeding the exciton Bohr radius, such as the samples under investigation in the present work, excitonic effects are suppressed due to charge separation [93], and nonexcitonic recombination (such as band-to-band and free-to bound transitions) may become dominant. Free-to-bound transitions are also known to have a significantly longer lifetime than band-to-band transitions [95]. A donor-to-free hole transition is thus consistent with both the energy and the lifetime of the low-energy line of our QWs.

Furthermore, interpreting the low-energy PL line of the N-polar MQWs as a donor-to-free hole transition offers not only an understanding of the spectral and temporal characteristic of this transition, but also for the absence of the splitting in the Ga-polar MQWs. In fact, the donor binding energy depends on the position of the donor relative to the QW interfaces, on the width of the QW, and, most importantly, on the polarity of the heterostructure [86]. The influence of polarity results from the difference in overlap between the electron and the ionized donor, which strongly depends on whether the electron resides at the donor interface or at the opposite one [this situation is exemplified in the band profiles shown as insets in Figs. 6(c)i and 6(c)iii]. In particular, for a donor located at the bottom interface of a 22-ML-wide N-polar (Ga-polar) $GaN/Al_{0.15}Ga_{0.85}N$ QW, a binding energy of 50 meV (20 meV) is obtained [86]. In other words, we would expect the free-to-bound transition to create a distinct doublet for the N-polar samples, but for the Ga-polar sample, the free-to-bound transition would be expected to spectrally overlap with the band-to-band transition.

The most abundant shallow donor in our structures is O. The preferential incorporation of O at the bottom interface (the "inverted" interface) is well documented for GaAs/(Al,Ga)As MQWs grown by MBE, and is attributed to the formation of an AlO_x floating layer during (Al,Ga)As growth [78,96]. It is very plausible that an analogous mechanism to preferentially incorporate O at the bottom interface is at work for GaN/(Al,Ga)N QWs as well. Overall, this hypothesis is the only one consistent with all experimental findings: the magnitude of the splitting for the N-polar samples, the long lifetime of the low-energy line, its saturation for high excitation density, and the absence of a detectable splitting for the Ga-polar samples.

D. Room-temperature photoluminescence

Figures 7(a)–7(b) show the normalized cw-PL spectra of the three pairs of samples acquired at room temperature. The PL signal is confirmed to originate from the QWs by comparison with the PL spectra of a sample free of QWs (not shown). The average intensity of the MQWs' cw PL is plotted in Fig. 7(c) and exhibits a nonmonotonous dependence on the width of the MQWs, which is more pronounced for the N-polar heterostructures. Interestingly, N-polar samples exhibit a higher luminescence intensity than Ga-polar ones, up to a factor 3 for the thickest QWs of the series.

Such enhanced radiative efficiency of the N-polar samples is further confirmed by observing the PL transients acquired at room temperature and as shown in Figs. 7(d)–7(e) for both polarities. The transients are fitted by monoexponential and biexponential decays for the Ga- and N-polar samples, respectively. The obtained characteristic times are plotted in Fig. 7(f) as a function of the QW width. The observed decay times are systematically shorter than that acquired at 10 K, which indicates that electron-hole recombination is predominantly nonradiative at room temperature [97], a phenomenon typically observed for such a type of heterostructure [87,88]. For the Ga-polar MQWs, the decay time of 0.1 ns has essentially no dependence on the widths of the individual QWs. In contrast, the decay times in the N-polar MQWs lengthen for larger wells, reaching up to 2 ns. This behavior is reminiscent of nonradiative recombination taking place at the interfaces of the QWs. The usual description of this decay channel by a characteristic time $\tau_{nr} = d/2S$ [98,99], with d the QW width and S the interface recombination velocity, is not applicable here since the out-of-plane location of carriers is primarily determined by the internal electric field and not by carrier diffusion. Instead, an exponential dependence of the decay time on the QW width is observed [$\tau_{nr} \propto \exp(d/L)$], with a characteristic length $L = 1$–2 nm, suggesting that the lifetime is controlled by the wave function overlap of spatially separated states.

In the following, we discuss the case where the point defects responsible for efficient nonradiative recombination in the Ga- and N-polar GaN/(Al,Ga)N QWs are

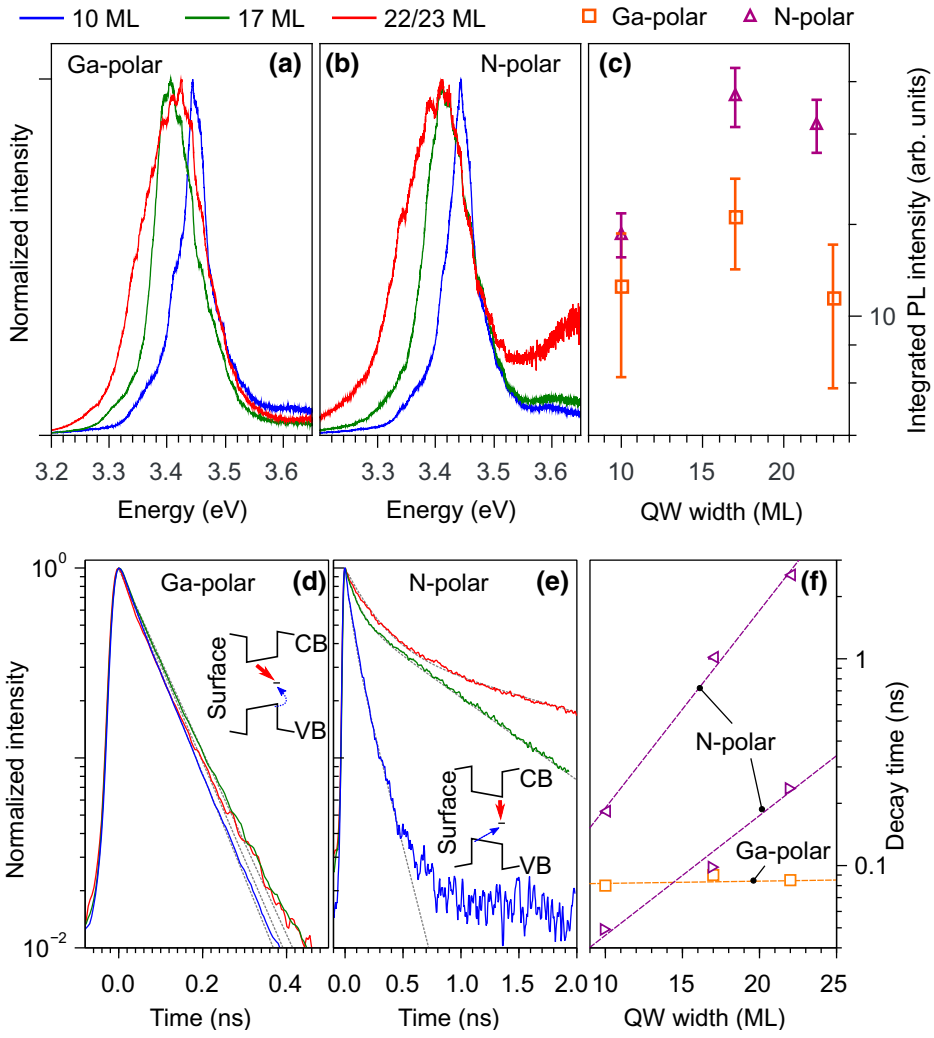

FIG. 7. Room-temperature PL of the three pairs of GaN/(Al,Ga)N MQWs. (a),(b) Normalized cw-PL spectra acquired with excitation at 244 nm with a power density of 50 kW/cm^2. (c) Integrated intensity of the GaN/(Al,Ga)N MQWs' cw PL between 3.15 and 3.6 eV. Error bars account for the dispersion at the scale of the sample. (d),(e) PL transients of the GaN/(Al,Ga)N MQWs. Dotted lines show the results of monoexponential and biexponential fits for the Ga- and N-polar samples, respectively. The insets depict a nonradiative decay path involving a hole trap state located at the bottom QW interface. Blue dotted (red plain) arrows refer to the decay of holes (electrons). (f) Nonradiative decay time extracted from the fits plotted as a function of the MQW width. Dashed lines are guides to the eye.

exclusively located at the bottom QW interface. The recombination scheme proposed in this scenario is schematized in the insets of Figs. 7(d) and 7(e). We further assume that the nonradiative recombination rate is limited by the trapping of minority carriers that are holes. As a matter of fact, in the Ga-polar samples, the excess of electrons is indeed substantial since the Fermi level intersects the bottom of the conduction band in each QW (see Fig. 8 in the Appendix). Under laser exposure, photoexcited holes in N-polar (Ga-polar) QWs are driven to the top (bottom) interface by the internal electric field. For the N-polar samples, the capture rate of holes by the traps located at the bottom interface should thus decrease exponentially with the well width due to the vanishing wave function overlap. In contrast, no dependence of the hole capture rate on the well width is expected for the Ga-polar samples. This simple consideration on the hole capture rate can thus account for the experimental observation that only N-polar samples exhibit a well-width-dependent nonradiative decay time.

Large densities of interface hole traps have been inferred in N-polar GaN/(Al,Ga)N heterostructures either grown by MOCVD [100] or MBE [101]. As a likely candidate, the N vacancy (V_N) was proposed, which forms two acceptorlike states in the bandgap of bulk GaN [102]. Ga-polar (In,Ga)N/GaN heterostructures grown by MOCVD are also expected to incorporate high densities of V_N [103]. For MOCVD growth, the current understanding is that V_N forms during high-temperature GaN growth where thermal GaN decomposition is non-negligible ($> 900\,^{\circ}C$), segregates at the surface even at low growth temperatures, and eventually incorporates in the bulk at the onset of (In,Ga)N growth [103–107]. Similarly, in N-polar GaN/(Al,Ga)N QWs grown by MOCVD, the presumed V_N forms at the onset of the ternary alloy growth (at the top QW interface) [100]. However, for MBE grown GaN/(Al,Ga)N QWs, the formation mechanism for V_N may differ. Another potential candidate for the trap state is the impurity Ca that was reported to act as a deep acceptor mediating efficient nonradiative recombination in (In,Ga)N QWs [22, 24]. In our case, the N-polar samples contain 10 times less Ca as the Ga-polar samples, which correlates with their enhanced radiative efficiency. Yet, *ab initio* calculations of bulk (In,Ga)N doped with Ca show that the electron capture coefficient of the deep state strongly decreases when increasing the band gap, becoming essentially zero above 2.8 eV [22].

We thus propose that the nonradiative recombination observed at room temperature for the GaN/(Al,Ga)N MQWs results from Shockley-Read-Hall recombination on point defects (presumably Ca or V_N) located at the bottom GaN QW interface. For N-polar heterostructures, this nonradiative process is significantly affected by the internal electric field. By increasing the QW width, the nonradiative recombination time is not constant but increases due to the reduction in the overlap between the electron and hole wavefunctions. Overall, the internal quantum efficiency is essentially given by the ratio between the nonradiative and radiative lifetimes. For the sample series under scrutiny, this ratio appears not to have a monotonous dependence on the QW width since the maximum PL intensity is observed for a QW width of 17 ML.

IV. SUMMARY AND CONCLUSIONS

Structurally equivalent Ga- and N-polar GaN/(Al,Ga)N MQWs are grown on freestanding GaN by PA MBE. Under optimized growth conditions, no more extended defects are found in the heterostructures than originally present in the substrates. Low concentrations of impurities are found in samples of opposite polarity, with the exception of Ca, which is measured with a 10 times higher concentration (8×10^{17} cm^{-3}) in the Ga-polar MQWs compared to the N-polar MQWs. At 10 K, the exciton decay within the MQWs is deduced to be predominantly radiative for all samples and the PL properties are entirely characterized by the QCSE. For the N-polar MQWs, an additional low-energy line is observed and ascribed to a free-to-bound recombination involving a shallow donor, likely O, aggregated at the QW bottom interface. At room temperature, the electron-hole pair recombination is governed by nonradiative processes for all samples. The decay rate in N-polar MQWs shows a dependence on the QW width and is lower than in Ga-polar MQWs. A nonradiative decay mediated by Shockley-Read-Hall recombination on deep states located at the bottom QW interface is proposed to account for these observations. Remarkably, the presence of internal electric fields is seen as beneficial in N-polar GaN/(Al,Ga)N MQWs for slowing down the nonradiative recombination. Nevertheless, further enhancement of the internal quantum efficiency of GaN/(Al,Ga)N heterostructures grown by MBE will necessarily require to minimize the density of point defects. Two approaches currently under development are the growth of dedicated buffer layers to bury point defects [103,108] and the use of different growth conditions [16,109].

ACKNOWLEDGMENTS

We are indebted to Katrin Morgenroth for her support during the preparation of the samples as well as for her dedicated maintenance of the MBE system together with Carsten Stemmler and Hans-Peter Schönherr. We thank Vladimir Kaganer for stimulating discussions concerning x-ray characterization and Manfred Ramsteiner for a critical reading of the manuscript. Funding from both the Bundesministerium für Bildung und Forschung through project FKZ:13N13662 and the Leibniz-Gemeinschaft under Grant No. SAW-2013-PDI-2 is gratefully acknowledged. Sergio Fernández-Garrido acknowledges the partial financial support received through the Spanish program Ramón y Cajal (co-financed by the European Social Fund)

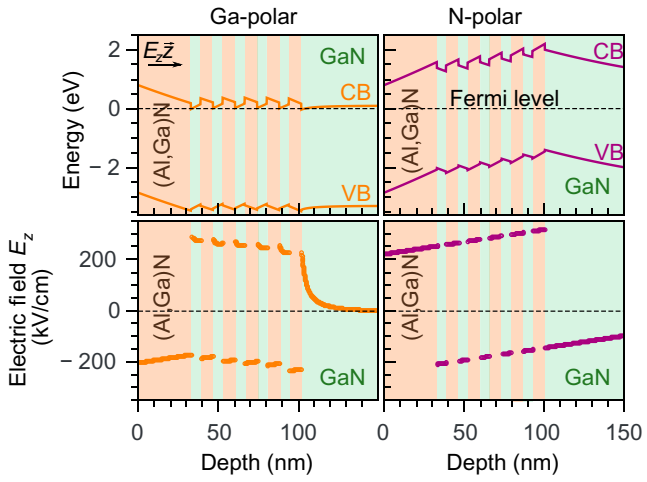

FIG. 8. Calculated conduction band (CB) and valence band (VB) structures and internal electric fields for the Ga- and N-polar 23/22 ML GaN/(Al,Ga)N MQWs.

under Grant No. RYC-2016-19509 from the former Ministerio de ciencia, innovación y universidades.

APPENDIX: CALCULATED BAND PROFILES

The band structure and electric field distribution obtained by Schrödinger-Poisson calculations of the thicker MQWs are plotted in Fig. 8. Clear differences can be observed between the Ga- and N-polar cases. In the first case, the Fermi level is located close to the conduction band minimum and the average internal electric field amounts to 280 kV/cm in the QWs. In the second case, the Fermi level is close to the midgap position and the average internal electric field amounts to 200 kV/cm within the QWs. In both cases, the electric field differs between each of the QWs of a MQW sample, with variations up to 15%.

[1] S. Y. Karpov and Y. N. Makarov, Dislocation effect on light emission efficiency in gallium nitride, Appl. Phys. Lett. **81**, 4721 (2002).

[2] K. Ban, J.-I. Yamamoto, K. Takeda, K. Ide, M. Iwaya, T. Takeuchi, S. Kamiyama, I. Akasaki, and H. Amano, Internal quantum efficiency of whole-composition-range AlGaN multiquantum wells, Appl. Phys Express **4**, 052101 (2011).

[3] A. Sampath, G. Garrett, E. Readinger, R. Enck, H. Shen, M. Wraback, J. Grandusky, and L. Schowalter, Characterization of nanometer scale compositionally inhomogeneous AlGaN active regions on bulk AlN substrates, Solid-State Electron. **54**, 1130 (2010), selected Papers from ISDRS 2009.

[4] S. F. Chichibu, A. Uedono, K. Kojima, H. Ikeda, K. Fujito, S. Takashima, M. Edo, K. Ueno, and S. Ishibashi, The origins and properties of intrinsic nonradiative recombination centers in wide bandgap GaN and AlGaN, J. Appl. Phys. **123**, 161413 (2018).

[5] H. Murotani, D. Akase, K. Anai, Y. Yamada, H. Miyake, and K. Hiramatsu, Dependence of internal quantum efficiency on doping region and Si concentration in Al-rich AlGaN quantum wells, Appl. Phys. Lett. **101**, 042110 (2012).

[6] Z. Bryan, I. Bryan, J. Xie, S. Mita, Z. Sitar, and R. Collazo, High internal quantum efficiency in AlGaN multiple quantum wells grown on bulk AlN substrates, Appl. Phys. Lett. **106**, 142107 (2015).

[7] M. Kneissl, T.-Y. Seong, J. Han, and H. Amano, The emergence and prospects of deep-ultraviolet light-emitting diode technologies, Nat. Photon. **13**, 233 (2019).

[8] B. S. Eller, J. Yang, and R. J. Nemanich, Electronic surface and dielectric interface states on GaN and AlGaN, J. Vac. Sci. Technol., A **31**, 050807 (2013).

[9] M. Huber, M. Silvestri, L. Knuuttila, G. Pozzovivo, A. Andreev, A. Kadashchuk, A. Bonanni, and A. Lundskog, Impact of residual carbon impurities and gallium vacancies on trapping effects in AlGaN/GaN metal insulator semiconductor high electron mobility transistors, Appl. Phys. Lett. **107**, 032106 (2015).

[10] A. Hu, C. Song, X. Yang, X. He, B. Shen, and X. Guo, Role of hole trapping in the unintentionally doped GaN layer in suppressing the two-dimensional electron gas degradation in AlGaN/GaN heterostructures on Si, Nanotechnology **30**, 314002 (2019).

[11] P. Dang, G. Khalsa, C. S. Chang, D. S. Katzer, N. Nepal, B. P. Downey, V. D. Wheeler, A. Suslov, A. Xie, E. Beam, Y. Cao, C. Lee, D. A. Muller, H. G. Xing, D. J. Meyer, and D. Jena, An all-epitaxial nitride heterostructure with concurrent quantum Hall effect and superconductivity, Sci. Adv. **7**, eabf1388 (2021).

[12] L. Lymperakis and J. Neugebauer, Large anisotropic adatom kinetics on nonpolar GaN surfaces: Consequences for surface morphologies and nanowire growth, Phys. Rev. B **79**, 241308(R) (2009).

[13] M. Sawicka, H. Turski, M. Siekacz, J. Smalc-Koziorowska, M. Kryśko, I. Dzięcielewski, I. Grzegory, and C. Skierbiszewski, Step-flow anisotropy of the *m*-plane gan $(1\bar{1}00)$ grown under nitrogen-rich conditions by plasma-assisted molecular beam epitaxy, Phys. Rev. B **83**, 245434 (2011).

[14] J. Shao, L. Tang, C. Edmunds, G. Gardner, O. Malis, and M. Manfra, Surface morphology evolution of m-plane $(1\bar{1}0)$ GaN during molecular beam epitaxy growth: Impact of Ga/N ratio, miscut direction, and growth temperature, J. Appl. Phys. **114**, 023508 (2013).

[15] M. Sawicka, P. Wolny, M. Kryśko, H. Turski, K. Szkudlarek, S. Grzanka, and C. Skierbiszewski, Comparative study of semipolar $(20\bar{2}1)$, nonpolar $(10\bar{1}0)$ and polar (0001) InGaN multi-quantum well structures grown under N- and In-excess by plasma assisted molecular beam epitaxy, J. Cryst. Growth **465**, 43 (2017).

[16] P. Tatarczak, H. Turski, K. P. Korona, E. Grzanka, C. Skierbiszewski, and A. Wysmołek, Optical properties of N-polar GaN: The possible role of nitrogen vacancy-related defects, Appl. Surf. Sci. **566**, 150734 (2021).

[17] O. Brandt, K. Kanamoto, M. Tsugami, T. Isu, and N. Tsukada, Comparative analysis of the optical quality of

single $In_{0.1}Ga_{0.9}As/Al_{0.33}Ga_{0.67}As$ quantum wells grown by molecular beam epitaxy on (100) and (311) GaAs substrates, Appl. Phys. Lett. **67**, 1885 (1995).

[18] A. J. Ptak, T. H. Myers, L. T. Romano, C. G. Van de Walle, and J. E. Northrup, Magnesium incorporation in GaN grown by molecular-beam epitaxy, Appl. Phys. Lett. **78**, 285 (2001).

[19] F. Tuomisto, K. Saarinen, B. Lucznik, I. Grzegory, H. Teisseyre, T. Suski, S. Porowski, P. R. Hageman, and J. Likonen, Effect of growth polarity on vacancy defect and impurity incorporation in dislocation-free GaN, Appl. Phys. Lett. **86**, 031915 (2005).

[20] C. Chèze, M. Siekacz, G. Muzioł, H. Turski, S. Grzanka, M. Kryśko, J. L. Weyher, M. Boćkowski, C. Hauswald, J. Lähnemann, O. Brandt, M. Albrecht, and C. Skierbiszewski, Investigation on the origin of luminescence quenching in N-polar (In, Ga)N multiple quantum wells, J. Vac. Sci. Technol. B **31**, 03C130 (2013).

[21] S. Fernández-Garrido, J. Lähnemann, C. Hauswald, M. Korytov, M. Albrecht, C. Chèze, C. Skierbiszewski, and O. Brandt, Comparison of the Luminous Efficiencies of Ga- and N-Polar $In_xGa_{1-x}N/In_yGa_{1-y}N$ Quantum Wells Grown by Plasma-Assisted Molecular Beam Epitaxy, Phys. Rev. Appl. **6**, 034017 (2016).

[22] J.-X. Shen, D. Wickramaratne, C. E. Dreyer, A. Alkauskas, E. Young, J. S. Speck, and C. G. Van de Walle, Calcium as a nonradiative recombination center in InGaN, Appl. Phys Express **10**, 021001 (2017).

[23] C. Chèze, F. Feix, J. Lähnemann, T. Flissikowski, M. Kryśko, P. Wolny, H. Turski, C. Skierbiszewski, and O. Brandt, Luminescent N-polar (In, Ga)N/GaN quantum wells achieved by plasma-assisted molecular beam epitaxy at temperatures exceeding 700°C, Appl. Phys. Lett. **112**, 022102 (2018).

[24] E. C. Young, N. Grandjean, T. E. Mates, and J. S. Speck, Calcium impurity as a source of non-radiative recombination in (In, Ga)N layers grown by molecular beam epitaxy, Appl. Phys. Lett. **109**, 212103 (2016).

[25] E. Sarigiannidou, E. Monroy, N. Gogneau, G. Radtke, P. Bayle-Guillemaud, E. Bellet-Amalric, B. Daudin, and J. L. Rouvière, Comparison of the structural quality in Ga-face and N-face polarity GaN/AlN multiple-quantum-well structures, Semicond. Sci. Technol. **21**, 612 (2006).

[26] F. Natali, Y. Cordier, J. Massies, S. Vezian, B. Damilano, and M. Leroux, Signature of monolayer and bilayer fluctuations in the width of (Al, Ga)N/GaN quantum wells, Phys. Rev. B **79**, 035328 (2009).

[27] J. Smalc-Koziorowska, M. Sawicka, T. Remmele, C. Skierbiszewski, I. Grzegory, and M. Albrecht, Mismatch relaxation by stacking fault formation of AlN islands in AlGaN/GaN structures on m-plane GaN substrates, Appl. Phys. Lett. **99**, 061901 (2011).

[28] B. Mazumder, M. H. Wong, C. A. Hurni, J. Y. Zhang, U. K. Mishra, and J. S. Speck, Asymmetric interfacial abruptness in N-polar and Ga-polar GaN/AlN/GaN heterostructures, Appl. Phys. Lett. **101**, 091601 (2012).

[29] J. Shao, D. N. Zakharov, C. Edmunds, O. Malis, and M. J. Manfra, Homogeneous AlGaN/GaN superlattices grown on free-standing $(11\bar{2}0)$ GaN substrates by plasma-assisted molecular beam epitaxy, Appl. Phys. Lett. **103**, 232103 (2013).

[30] M. N. Fireman, B. Bonef, E. C. Young, N. Nookala, M. A. Belkin, and J. S. Speck, Strain compensated superlattices on m-plane gallium nitride by ammonia molecular beam epitaxy, J. Appl. Phys. **122**, 075105 (2017).

[31] E. Kuokstis, C. Q. Chen, M. E. Gaevski, W. H. Sun, J. W. Yang, G. Simin, M. A. Khan, H. P. Maruska, D. W. Hill, M. C. Chou, J. J. Gallagher, and B. Chai, Polarization effects in photoluminescence of c- and m-plane GaN/AlGaN multiple quantum wells, Appl. Phys. Lett. **81**, 4130 (2002).

[32] Z. Vashaei, C. Bayram, P. Lavenus, and M. Razeghi, Photoluminescence characteristics of polar and nonpolar AlGaN/GaN superlattices, Appl. Phys. Lett. **97**, 121918 (2010).

[33] S. Keller, N. Pfaff, S. P. DenBaars, and U. K. Mishra, Polarization spectroscopy of N-polar AlGaN/GaN multi quantum wells grown on vicinal $(000\bar{1})$ GaN, Appl. Phys. Lett. **101**, 182103 (2012).

[34] R. G. Banal, Y. Taniyasu, and H. Yamamoto, Deep-ultraviolet light emission properties of nonpolar m-plane AlGaN quantum wells, Appl. Phys. Lett. **105**, 053104 (2014).

[35] D. Rosales, B. Gil, T. Bretagnon, B. Guizal, N. Izyumskaya, M. Monavarian, F. Zhang, S. Okur, V. Avrutin, U. Özgür, and H. Morkoç, Recombination dynamics of excitons with low non-radiative component in semi-polar $(10\bar{1}1)$-oriented GaN/AlGaN multiple quantum wells, J. Appl. Phys. **116**, 093517 (2014).

[36] M. H. Wong, S. Keller, S. D. Nidhi, D. J. Denninghoff, S. Kolluri, D. F. Brown, J. Lu, N. A. Fichtenbaum, E. Ahmadi, U. Singisetti, A. Chini, S. Rajan, S. P. DenBaars, J. S. Speck, and U. K. Mishra, N-polar GaN epitaxy and high electron mobility transistors, Semicond. Sci. Technol. **28**, 074009 (2013).

[37] F. Akyol, D. N. Nath, E. Gür, P. S. Park, and S. Rajan, N-polar III–nitride green (540 nm) light emitting diode, Jpn. J. Appl. Phys. **50**, 052101 (2011).

[38] S.-H. Han, D.-Y. Lee, J.-Y. Lim, J. W. Lee, D.-J. Kim, Y. S. Kim, S.-T. Kim, and S.-J. Park, Effect of internal electric field in well layer of InGaN/GaN multiple quantum well light-emitting diodes on efficiency droop, Jpn. J. Appl. Phys. **51**, 100201 (2012).

[39] K. Dong, D. Chen, B. Liu, H. Lu, P. Chen, R. Zhang, and Y. Zheng, Characteristics of polarization-doped N-face III-nitride light-emitting diodes, Appl. Phys. Lett. **100**, 073507 (2012).

[40] S.-W. Feng, P.-H. Liao, B. Leung, J. Han, F.-W. Yang, and H.-C. Wang, Efficient carrier relaxation and fast carrier recombination of N-polar InGaN/GaN light emitting diodes, J. Appl. Phys. **118**, 043104 (2015).

[41] Z. Q. Li, M. Lestradet, Y. G. Xiao, and S. Li, Effects of polarization charge on the photovoltaic properties of InGaN solar cells, Phys. Status Solidi A **208**, 928 (2010).

[42] J. Zúñiga Pérez, V. Consonni, L. Lymperakis, X. Kong, A. Trampert, S. Fernández-Garrido, O. Brandt, H. Renevier, S. Keller, K. Hestroffer, M. R. Wagner, J. S. Reparaz, F. Akyol, S. Rajan, S. Rennesson, T. Palacios, and G. Feuillet, Polarity in GaN and ZnO: Theory, measurement, growth, and devices, Appl. Phys. Rev. **3**, 041303 (2016).

[43] B. Heying, R. Averbeck, L. F. Chen, E. Haus, H. Riechert, and J. S. Speck, Control of GaN surface morphologies

using plasma-assisted molecular beam epitaxy, J. Appl. Phys. **88**, 1855 (2000).

[44] D. F. Storm, D. J. Meyer, D. S. Katzer, S. C. Binari, T. Paskova, E. A. Preble, K. R. Evans, L. Zhou, and D. J. Smith, Homoepitaxial N-polar GaN layers and HEMT structures grown by rf-plasma assisted molecular beam epitaxy, J. Vac. Sci. Technol. B **30**, 02B113 (2012).

[45] D. Storm, T. McConkie, D. Katzer, B. Downey, M. Hardy, D. Meyer, and D. J. Smith, Effect of interfacial oxygen on the microstructure of MBE-grown homoepitaxial N-polar GaN, J. Cryst. Growth **409**, 14 (2015).

[46] D. Storm, M. Hardy, D. Katzer, N. Nepal, B. Downey, D. Meyer, T. O. McConkie, L. Zhou, and D. J. Smith, Critical issues for homoepitaxial GaN growth by molecular beam epitaxy on hydride vapor-phase epitaxy-grown GaN substrates, J. Cryst. Growth **456**, 121 (2016), proceeding of the 9th International Workshop on Bulk Nitride Semiconductors.

[47] P. Blanchard, M. Brubaker, T. Harvey, A. Roshko, N. Sanford, J. Weber, and K. Bertness, Characterization of sub-monolayer contaminants at the regrowth interface in GaN nanowires grown by selective-area molecular beam epitaxy, Crystals **8**, 178 (2018).

[48] C. Chèze, M. Sawicka, M. Siekacz, H. Turski, G. Cywiński, J. Smalc-Koziorowska, J. L. Weyher, M. Kryśko, B. Łucznik, M. Boćkowski, and C. Skierbiszewski, Step-flow growth mode instability of N-polar GaN under N-excess, Appl. Phys. Lett. **103**, 071601 (2013).

[49] H. Okumura, B. M. McSkimming, T. Huault, C. Chaix, and J. S. Speck, Growth diagram of N-face GaN $(000\bar{1})$ grown at high rate by plasma-assisted molecular beam epitaxy, Appl. Phys. Lett. **104**, 012111 (2014).

[50] G. Koblmüller, R. Averbeck, H. Riechert, and P. Pongratz, Direct observation of different equilibrium Ga adlayer coverages and their desorption kinetics on GaN (0001) and $(000\bar{1})$ surfaces, Phys. Rev. B **69**, 035325 (2004).

[51] P. Hacke, G. Feuillet, H. Okumura, and S. Yoshida, Monitoring surface stoichiometry with the (2×2) reconstruction during growth of hexagonal-phase GaN by molecular beam epitaxy, Appl. Phys. Lett. **69**, 2507 (1996).

[52] N. Gogneau, D. Jalabert, E. Monroy, E. Sarigiannidou, J. L. Rouvière, T. Shibata, M. Tanaka, J. M. Gerard, and B. Daudin, Influence of AlN overgrowth on structural properties of GaN quantum wells and quantum dots grown by plasma-assisted molecular beam epitaxy, J. Appl. Phys. **96**, 1104 (2004).

[53] A. V. Kuchuk, V. P. Kladko, T. L. Petrenko, V. P. Bryksa, A. E. Belyaev, Y. I. Mazur, M. E. Ware, E. A. DeCuir, and G. J. Salamo, Mechanism of strain-influenced quantum well thickness reduction in GaN/AlN short-period superlattices, Nanotechnology **25**, 245602 (2014).

[54] E. Iliopoulos and T. D. Moustakas, Growth kinetics of AlGaN films by plasma-assisted molecular-beam epitaxy, Appl. Phys. Lett. **81**, 295 (2002).

[55] O. Brandt, P. Waltereit, and K. H. Ploog, Determination of strain state and composition of highly mismatched group-III nitride heterostructures by x-ray diffraction, J. Phys. D: Appl. Phys. **35**, 577 (2002).

[56] G. Snider, 1D Poisson/Schroedinger, University of Notre Dame, https://www3.nd.edu/ gsnider.

[57] B. Heying, E. J. Tarsa, C. R. Elsass, P. Fini, S. P. DenBaars, and J. S. Speck, Dislocation mediated surface morphology of GaN, J. Appl. Phys. **85**, 6470 (1999).

[58] Y. Cho, S. Sadofev, S. Fernández-Garrido, R. Calarco, H. Riechert, Z. Galazka, R. Uecker, and O. Brandt, Impact of substrate nitridation on the growth of InN on In2O3(111) by plasma-assisted molecular beam epitaxy, Appl. Surf. Sci. **369**, 159 (2016).

[59] H. Turski, F. Krzyżewski, A. Feduniewicz-Żmuda, P. Wolny, M. Siekacz, G. Muziol, C. Chéze, K. Nowakowski-Szukudlarek, H. G. Xing, D. Jena, M. Załuska-Kotur, and C. Skierbiszewski, Unusual step meandering due to Ehrlich-Schwoebel barrier in GaN epitaxy on the N-polar surface, Appl. Surf. Sci. **484**, 771 (2019).

[60] S. Diez, S. Mohanty, C. Kurdak, and E. Ahmadi, Record high electron mobility and low sheet resistance on scaled-channel N-polar GaN/AlN heterostructures grown on on-axis N-polar GaN substrates by plasma-assisted molecular beam epitaxy, Appl. Phys. Lett. **117**, 042102 (2020).

[61] G. Koblmüller, F. Reurings, F. Tuomisto, and J. S. Speck, Influence of Ga/N ratio on morphology, vacancies, and electrical transport in GaN grown by molecular beam epitaxy at high temperature, Appl. Phys. Lett. **97**, 191915 (2010).

[62] C. Misbah, O. Pierre-Louis, and Y. Saito, Crystal surfaces in and out of equilibrium: A modern view, Rev. Mod. Phys. **82**, 981 (2010).

[63] V. M. Kaganer, B. Jenichen, M. Ramsteiner, U. Jahn, C. Hauswald, F. Grosse, S. Fernández-Garrido, and O. Brandt, Quantitative evaluation of the broadening of x-ray diffraction, raman, and photoluminescence lines by dislocation-induced strain in heteroepitaxial GaN films, J. Phys. D: Appl. Phys. **48**, 385105 (2015).

[64] L. Rigutti, L. Mancini, W. Lefebvre, J. Houard, D. Hernàndez-Maldonado, E. D. Russo, E. Giraud, R. Butté, J.-F. Carlin, N. Grandjean, D. Blavette, and F. Vurpillot, Statistical nanoscale study of localised radiative transitions in GaN/AlGaN quantum wells and AlGaN epitaxial layers, Semicond. Sci. Technol. **31**, 095009 (2016).

[65] B. Bonef, M. Lopez-Haro, L. Amichi, M. Beeler, A. Grenier, E. Robin, P.-H. Jouneau, N. Mollard, I. Mouton, B. Haas, E. Monroy, and C. Bougerol, Composition analysis of III-nitrides at the nanometer scale: Comparison of energy dispersive x-ray spectroscopy and atom probe tomography, Nanoscale Res. Lett. **11**, 461 (2016).

[66] Z. Wasilewski, S. Rolfe, and R. Wilson, Contamination in molecular beam epitaxy: The role of arsenic drag effect, J. Cryst. Growth. **175-176**, 1270 (1997).

[67] N. Grandjean, M. Leroux, J. Massies, M. Mesrine, and M. Laügt, Molecular beam epitaxy of GaN under N-rich conditions using NH_3, Jpn. J. Appl. Phys. **38**, 618 (1999).

[68] L. K. Li, M. J. Jurkovic, W. I. Wang, J. M. V. Hove, and P. P. Chow, Surface polarity dependence of Mg doping in GaN grown by molecular-beam epitaxy, Appl. Phys. Lett. **76**, 1740 (2000).

[69] H. Kim, F. J. Fälth, and T. G. Andersson, Unintentional incorporation of B, As, and O impurities in GaN grown

by molecular beam epitaxy, J. Electron. Mater. **30**, 1343 (2001).
[70] H. M. Ng and A. Y. Cho, Investigation of Si doping and impurity incorporation dependence on the polarity of GaN by molecular beam epitaxy, J. Vac. Sci. Technol. B **20**, 1217 (2002).
[71] M. Sumiya, K. Yoshimura, K. Ohtsuka, and S. Fuke, Dependence of impurity incorporation on the polar direction of GaN film growth, Appl. Phys. Lett. **76**, 2098 (2000).
[72] G. Popovici, W. Kim, A. Botchkarev, H. Tang, H. Morkoç, and J. Solomon, Impurity contamination of GaN epitaxial films from the sapphire, SiC and ZnO substrates, Appl. Phys. Lett. **71**, 3385 (1997).
[73] J. D. Ferguson, M. A. Reshchikov, A. A. Baski, J. K. Hite, M. A. Mastro, and C. R. Eddy Jr., Determination of GaN polarity on periodically oriented surfaces, J. Vac. Sci. Technol. B **33**, 011206 (2015).
[74] T. K. Zywietz, J. Neugebauer, and M. Scheffler, The adsorption of oxygen at GaN surfaces, Appl. Phys. Lett. **74**, 1695 (1999).
[75] T. Mattila and R. M. Nieminen, Point-defect complexes and broadband luminescence in GaN and AlN, Phys. Rev. B **55**, 9571 (1997).
[76] L. Ramos, J. Furthmüller, L. Scolfaro, J. Leite, and F. Bechstedt, Substitutional carbon in group-iii nitrides: Ab initio description of shallow and deep levels, Phys. Rev. B **66**, 075209 (2002).
[77] T. Achtnich, G. Burri, M. A. Py, and M. Ilegems, Secondary ion mass spectrometry study of oxygen accumulation at GaAs/AlGaAs interfaces grown by molecular beam epitaxy, Appl. Phys. Lett. **50**, 1730 (1987).
[78] T. Achtnich, G. Burri, and M. Ilegems, Study of oxygen incorporation in AlGaAs layers grown by molecular beam epitaxy, J. Vac. Sci. Technol. A **7**, 2537 (1989).
[79] P. Lefebvre, J. Allègre, B. Gil, A. Kavokine, H. Mathieu, W. Kim, A. Salvador, A. Botchkarev, and H. Morkoç, Recombination dynamics of free and localized excitons in GaN/$Ga_{0.93}Al_{0.07}N$ quantum wells, Phys. Rev. B **57**, R9447 (1998).
[80] N. Grandjean, B. Damilano, J. Massies, G. Neu, M. Teissere, I. Grzegory, S. Porowski, M. Gallart, P. Lefebvre, B. Gil, and M. Albrecht, Optical properties of GaN epilayers and GaN/AlGaN quantum wells grown by molecular beam epitaxy on GaN(0001) single crystal substrate, J. Appl. Phys. **88**, 183 (2000).
[81] M. Gallart, A. Morel, T. Taliercio, P. Lefebvre, B. Gil, J. Allègre, H. Mathieu, N. Grandjean, M. Leroux, and J. Massies, Scale effects on exciton localization and nonradiative processes in GaN/AlGaN quantum wells, Phys. Status Solidi A **180**, 127 (2000).
[82] B. Chwalisz, A. Wysmolek, K. P. Korona, R. Stępniewski, C. Skierbiszewski, I. Grzegory, and S. Porowski, Anomalous behaviour of the photoluminescence from GaN/AlGaN quantum wells, Phys. Status Solidi C **2**, 1010 (2005).
[83] T. Bretagnon, P. Lefebvre, P. Valvin, R. Bardoux, T. Guillet, T. Taliercio, B. Gil, N. Grandjean, F. Semond, B. Damilano, A. Dussaigne, and J. Massies, Radiative lifetime of a single electron-hole pair in GaN/AlN quantum dots, Phys. Rev. B **73**, 113304 (2006).
[84] C. E. Dreyer, A. Janotti, C. G. Van de Walle, and D. Vanderbilt, Correct Implementation of Polarization Constants in Wurtzite Materials and Impact on III-Nitrides, Phys. Rev. X **6**, 021038 (2016).
[85] P. Reddy, I. Bryan, Z. Bryan, J. Tweedie, S. Washiyama, R. Kirste, S. Mita, R. Collazo, and Z. Sitar, Charge neutrality levels, barrier heights, and band offsets at polar AlGaN, Appl. Phys. Lett. **107**, 091603 (2015).
[86] A. Morel, P. Lefebvre, T. Taliercio, M. Gallart, B. Gil, and H. Mathieu, Donor binding energies in group III-nitride-based quantum wells: Influence of internal electric fields, Mater. Sci. Semicond. Process. **82**, 221 (2001).
[87] M. Smith, J. Y. Lin, H. X. Jiang, A. Salvador, A. Botchkarev, W. Kim, and H. Morkoç, Optical transitions in GaN/$Al_xGa_{1-x}N$ multiple quantum wells grown by molecular beam epitaxy, Appl. Phys. Lett. **69**, 2453 (1996).
[88] K. C. Zeng, J. Li, J. Y. Lin, and H. X. Jiang, Optimizing growth conditions for GaN/$Al_xGa_{1-x}N$ multiple quantum well structures, Appl. Phys. Lett. **76**, 864 (2000).
[89] M. Gallart, P. Lefebvre, A. Morel, T. Taliercio, B. Gil, J. Allègre, H. Mathieu, B. Damilano, N. Grandjean, and J. Massies, Reduction of carrier in-plane mobility in group-III nitride based quantum wells: The role of internal electric fields, Phys. Status Solidi A **183**, 61 (2001).
[90] H. Haratizadeh, B. Monemar, P. P. Paskov, P. O. Holtz, E. Valcheva, P. Persson, M. Iwaya, S. Kamiyama, H. Amano, and I. Akasaki, Optical observation of discrete well width fluctuations in wide band gap III-nitride quantum wells, Phys. Status Solidi B **244**, 1727 (2007).
[91] Y. Hayakawa, T. Fukuno, K. Nakamura, H. Miyake, K. Hiramatsu, and Y. Yamada, Binding energy of localized biexcitons in AlGaN-based quantum wells, Appl. Phys. Express **7**, 122101 (2014).
[92] F. Stokker-Cheregi, A. Vinattieri, E. Feltin, D. Simeonov, J.-F. Carlin, R. Butté, N. Grandjean, and M. Gurioli, Biexciton kinetics in GaN quantum wells: Time-resolved and time-integrated photoluminescence measurements, Phys. Rev. B **77**, 125342 (2008).
[93] F. Stokker-Cheregi, A. Vinattieri, E. Feltin, D. Simeonov, J. Levrat, J.-F. Carlin, R. Butté, N. Grandjean, and M. Gurioli, Impact of quantum confinement and quantum confined Stark effect on biexciton binding energy in GaN/AlGaN quantum wells, Appl. Phys. Lett. **93**, 152105 (2008).
[94] C. He, Z. Qin, F. Xu, M. Hou, S. Zhang, L. Zhang, X. Wang, W. Ge, and B. Shen, Free and bound excitonic effects in $Al_{0.5}Ga_{0.5}N/Al_{0.35}Ga_{0.65}N$ MQWs with different Si-doping levels in the well layers, Sci. Rep. **5**, 13046 (2015).
[95] G. Balchin, L. Smith, A. Petrou, and B. McCombe, Time-resolved polarized photoluminescence spectroscopy of confined donors in GaAs/$Al_xGa_{1-x}As$ quantum wells, Superlattices Microstruct. **18**, 291 (1995).
[96] N. Chand, Growth of high quality AlGaAs/GaAs heterostructures by molecular beam epitaxy for photonic and electronic device applications, Thin Solid Films **231**, 143 (1993).
[97] L. C. Andreani, F. Tassone, and F. Bassani, Radiative lifetime of free excitons in quantum wells, Solid State Commun. **77**, 641 (1991).

[98] R. J. Nelson and R. G. Sobers, Interfacial recombination velocity in GaAlAs/GaAs heterostructures, Appl. Phys. Lett. **32**, 761 (1978).

[99] D. J. Wolford, G. D. Gilliland, T. F. Kuech, J. F. Klem, H. P. Hjalmarson, J. A. Bradley, C. F. Tsang, and J. Martinsen, Comparison of transport, recombination, and interfacial quality in molecular beam epitaxy and organometallic vapor phase epitaxy GaAs/$Al_xGa_{1-x}As$ structures, Appl. Phys. Lett. **64**, 1416 (1994).

[100] V. Prozheeva, I. Makkonen, H. Li, S. Keller, U. K. Mishra, and F. Tuomisto, Interfacial N Vacancies in GaN/(Al, Ga)N/GaN Heterostructures, Phys. Rev. Appl. **13**, 044034 (2020).

[101] S. Mohanty, S. Diez, Z. A. Jian, and E. Ahmadi, Design of ultra-scaled-channel N-polar GaN HEMTs with high charge density: A systematic study of hole traps and their impact on charge density in the channel, J. Appl. Phys. **128**, 235701 (2020).

[102] J. L. Lyons and C. G. Van de Walle, Computationally predicted energies and properties of defects in GaN, Npj Comput. Mater. **3**, 12 (2017).

[103] Y. Chen, C. Haller, W. Liu, S. Y. Karpov, J.-F. Carlin, and N. Grandjean, GaN buffer growth temperature and efficiency of InGaN/GaN quantum wells: The critical role of nitrogen vacancies at the GaN surface, Appl. Phys. Lett. **118**, 111102 (2021).

[104] T. Akasaka, H. Gotoh, T. Saito, and T. Makimoto, High luminescent efficiency of InGaN multiple quantum wells grown on InGaN underlying layers, Appl. Phys. Lett. **85**, 3089 (2004).

[105] A. M. Armstrong, B. N. Bryant, M. H. Crawford, D. D. Koleske, S. R. Lee, and J. J. Wierer, Defect-reduction mechanism for improving radiative efficiency in InGaN/GaN light-emitting diodes using InGaN underlayers, J. Appl. Phys. **117**, 134501 (2015).

[106] C. Haller, J.-F. Carlin, G. Jacopin, D. Martin, R. Butté, and N. Grandjean, Burying non-radiative defects in InGaN underlayer to increase InGaN/GaN quantum well efficiency, Appl. Phys. Lett. **111**, 262101 (2017).

[107] C. Haller, J.-F. Carlin, G. Jacopin, W. Liu, D. Martin, R. Butté, and N. Grandjean, GaN surface as the source of non-radiative defects in InGaN/GaN quantum wells, Appl. Phys. Lett. **113**, 111106 (2018).

[108] R. Chaudhuri, Z. Chen, D. A. Muller, H. G. Xing, and D. Jena, High-conductivity polarization-induced 2D hole gases in undoped GaN/AlN heterojunctions enabled by impurity blocking layers, J. Appl. Phys. **130**, 025703 (2021).

[109] J. Wang, K. F. Jorgensen, E. Farzana, K. S. Qwah, M. Monavarian, Z. J. Biegler, T. Mates, and J. S. Speck, Impact of growth parameters on the background doping of GaN films grown by ammonia and plasma-assisted molecular beam epitaxy for high-voltage vertical power switches, APL Mater. **9**, 081118 (2021).